



Article

Investigation into Red Emission and Its Applications: Solvatochromic N-Doped Red Emissive Carbon Dots with Solvent Polarity Sensing and Solid-State Fluorescent Nanocomposite Thin Films

Justin B. Domena ¹, Ermin Celebic ¹, Braulio C. L. B. Ferreira ¹, Yiqun Zhou ¹, Wei Zhang ¹, Jiuyan Chen ¹, M. Bartoli ², A. Tagliaferro ², Qiaxian Johnson ³, Bhanu P. S. Chauhan ³, Victor Paulino ¹, Jean-Hubert Olivier ¹ and Roger M. Leblanc ¹,*

- ¹ Department of Chemistry, University of Miami, Coral Gables, FL 33146, USA
- ² Department of Applied Science and Technology, Politecnico di Torino, 10129 Torino, Italy
- Department of Chemistry, William Paterson University of New Jersey, 300 Pompton Rd, Wayne, NJ 07470, USA
- * Correspondence: rml@miami.edu

Abstract: In this work, a NIR emitting dye, *p*-toluenesulfonate (IR-813) was explored as a model precursor to develop red emissive carbon dots (813-CD) with solvatochromic behavior with a red-shift observed with increasing solvent polarity. The 813-CDs produced had emission peaks at 610 and 698 nm, respectively, in water with blue shifts of emission as solvent polarity decreased. Subsequently, 813-CD was synthesized with increasing nitrogen content with polyethyleneimine (PEI) to elucidate the change in band gap energy. With increased nitrogen content, the CDs produced emissions as far as 776 nm. Additionally, a CD nanocomposite polyvinylpyrrolidone (PVP) film was synthesized to assess the phenomenon of solid-state fluorescence. Furthermore, the CDs were found to have electrochemical properties to be used as an additive doping agent for PVP film coatings.

Keywords: carbon dots; red emission; solvatochromic; nanocomposite; thin film



Citation: Domena, J.B.; Celebic, E.; Ferreira, B.C.L.B.; Zhou, Y.; Zhang, W.; Chen, J.; Bartoli, M.; Tagliaferro, A.; Johnson, Q.; Chauhan, B.P.S.; et al. Investigation into Red Emission and Its Applications: Solvatochromic N-Doped Red Emissive Carbon Dots with Solvent Polarity Sensing and Solid-State Fluorescent Nanocomposite Thin Films. *Molecules* 2023, 28, 1755. https://doi.org/10.3390/molecules 28041755

Academic Editor: Zhaohui Li

Received: 22 January 2023 Revised: 8 February 2023 Accepted: 10 February 2023 Published: 12 February 2023



Copyright: © 2023 by the authors. Licensee MDPI, Basel, Switzerland. This article is an open access article distributed under the terms and conditions of the Creative Commons Attribution (CC BY) license (https://creativecommons.org/licenses/by/4.0/).

1. Introduction

Carbon dots (CDs) have attracted increased attention in various biomedical areas such as in vitro/in vivo imaging, photodynamic and photothermal therapy [1–7]. When compared to typical organic dyes, CDs have the advantage of low cost, high biocompatibility and photostability, and amphiphilic behaviors [8–11]. Current efforts in developing red-emissive carbon dots as photosensitizers (PS) past 650 nm have been elusive [12]. The importance of this photophysical property is to surpass the requirement of the utilization of light within the red region to NIR-I window ranging between 650-950 nm, respectively for enhanced biological imaging [13,14]. A multitude of studies have sought to elucidate the synthetic methods to reach red emissive CDs, though few reach past the far-red region. Such efforts involve using carbon sources with features such as extended aromatic systems or heteroatoms (sulfur, nitrogen, and phosphorus) [15–22]. Specifically, the presence of heterocycles has been deduced to contribute to an increased degree of surface defects which effectively reduces the HOMO-LUMO energy gaps leading to a bathochromic shift of emission. In this study, we investigated the increased doping of nitrogen of 813-CDs by the introduction of different chain length PEI. To investigate the electronic transitions of the 813 CDs, the optical band gap energies of the respective CDs were elucidated by using the UV-vis spectrum converted to α vs energy plot by using Equation (1) instead of Tauc's plot.

$$\alpha = \frac{2.303 A}{l} \tag{1}$$

Molecules **2023**, 28, 1755 2 of 18

where α is denoted as the molar absorption coefficient at the resultant wavelength and is calculated from Beer-Lambert's relation according to Equation (1) such that A is the absorbance and l is the optical pathlength. The simple use of the Tauc approach is incorrect due to its applicability only to crystals, while CDs should be correctly modelled as large molecules [23–25]. Studies have suggested that intricate surface modifications are vital to develop red emissive CDs. Additionally, the interest in developing novel CDs from NIR dye sources has increased greatly [26]. This is due to the notion that when synthesizing a CD, the precursor is only partially broken down during the reaction, leaving moieties close to that of the original base structure. Hence, most of the conjugated network is retained resulting in a slight hypsochromic shift. As promising candidates, NIR fluorophores as precursors to red emissive CDs are of interest.

Until recently, post-synthetic parameters have been investigated to understand the influence of solvent polarity on the emissive properties of CDs [27–34]. Solvents of various polarities have discreet effects on the electronic transition of dipolar solutes. For example, when exposed to highly polar solvent, a fluorophore can exhibit two types of solvatochromism (positive or negative) [35,36]. Positive solvatochromism occurs due to a lower shift in the UV-vis transition energy resulting in a longer wavelength. This phenomenon is observed because the dipole moment of the molecule in ground state is smaller than that of the dipole moment in the excited state [37]. On the other hand, fluorophores exhibit negative solvatochromism due to a higher shift of UV-vis transition energy resulting in a shorter wavelength [38]. In this work, we propose that this feature of solvent polarity is important as CDs can be exploited in two ways: to produce a red shift in its optical properties, and to be used as a polarity sensing agent. Herein, we report the development of stable red emitting 813-CDs with polarity sensing capabilities.

Polyvinylpyrrolidone (PVP) has extensively been studied for its application in pharmaceuticals, electronics, cosmetics, and polymers [39–45]. Specifically, as a thin film composite, PVP, when polymerized with CDs, may have the feature to lock in place their emissive state [46–49], resulting in what is known as solid state fluorescence. There are few papers which address this phenomenon as carbon dots typically undergo fluorescence self-quenching in solid state due to aggregation [50,51]. Furthermore, these 813-CDs have been used with PVP to develop a red emitting thin film nanocomposite polymer which exhibits solid state fluorescence. We hypothesize that by introducing the CDs into a polymer matrix, the disabling of both the π – π interaction and fluorescence resonance energy transfer (FRET) between neighboring CDs will be observed. These interactions are known to play a key role in fluorescence self-quenching of CDs in solid state. Another promising feature of CDs is their potential as a doping agent to enhance electrochemical behaviors in PVP films, namely coatings for battery cathodes.

Herein, we propose the synthesis of far-red emitting carbon dots from the NIR emitting dye, IR-813. In comparison to current NIR photosensitizers, CDs boast features such as thermal and photostability. The feature of these carbon dots stems from the passivation of PEI during synthesis which aids in two aspects: (1) to have increased water solubility, as carbon dots derived from dyes usually lack this characteristic; and (2) PEI as a polymer encases the dye during microwave irradiation to slow the thermal degradation of the dye [52]. A feature of CDs to be used biologically is dependent on their surface functionalization. Specifically, the surface of the CD can modulate the pathway of cellular uptake, intracellular trafficking, and cytotoxicity [53]. As a surface passivant, PEI is a highly favored cationic macromolecule for use in gene transfer therapy due to high transfection efficiency [54]. Additionally, PEI molecules interact with negatively charged proteins in cytoskeletons, such as actin and beta-tubulin [55]. Another important feature of selecting PEI for surface functionalization of CDs is to provide both a positive charge and to improve permeabilization of the plasma membrane. The literature further conjectures that PEI as a drug delivery vesicle or passivant can disrupt endosomal membranes through the well-known "proton sponge effect", which states that the presence of a weekly basic molecule may cause the endosome to burst. This facilitates the possible pathways that allow binding of the material

Molecules **2023**, 28, 1755 3 of 18

to DNA [56,57]. To further clarify our rationale for PEI as a choice for nitrogen content, the literature shows that the increase of PEI weight during synthesis serves as a facile method to increase the degree of amidation of a nanoparticle [58].

2. Experimental Section

2.1. Materials

Two polyethyleneimine (PEI), branched (MW: 600 and 25 K) and p-toluenesulfonate were procured from Sigma-Aldrich (St. Louis, MO, USA). Polyvinylpyrrolidone (PVP) was obtained from VWR (West Chester, PA, USA). All solvents used were HPLC grade including ethanol, acetic acid, dimethyl sulfoxide (DMSO), dimethylformamide (DMF), methylene chloride, chloroform, ethyl acetate, toluene, ether, and hexane which were purchased from Sigma-Aldrich (St. Louis, MO, USA), and were used as received without further purification. Deionized (DI) water used was ultrapure (type I) water which was purified using a Millipore Direct-Q 3 water purification system acquired from EMD Millipore Corporation. The purified water displayed a surface tension of 72.6 mN m $^{-1}$, a resistivity of 18.2 MW cm and a pH value of 7.0 \pm 0.3 at 20.0 \pm 0.5 °C. All the chemicals were used as received.

2.2. Synthesis of 813-CD-600 PEI

The 813-CDs were obtained by means of microwave pyrolysis of IR813 (0.100 g) and PEI MW 600 (0.050 g) as illustrated in Figure S1 (in the Supplementary Materials). To preface, the precursors were dispersed in a beaker containing 15 mL of methanol and sonicated for 1 min to ensure a homogenous mixture which was observed to exhibit a dark-green color. The solution of starting material was then placed in the microwave and set for 360 s at a power setting of 700 W. Post pyrolysis, it was observed that no solution remained, leaving a bright orange gel-like product, 813-CD (Figure S2A). The product was then purified by flash chromatography with an eluent system of 75% hexane, 5% methanol, and 20% ethyl acetate by volume (v:v:v), producing an orange-red product labelled 813-CD-600 PEI. To ensure a product with little to no solvent, a Buchi Rotavapor (Waterbath B-480) was used to eliminate all organic solvent impurities. The purified solution of 813-CDs was dried and re-dispersed in ultrapure (type I) deionized (DI) water. The dispersion was then frozen at $-40\,^{\circ}\text{C}$ for 24 h and sequentially set for lyophilization for 72 h. Producing again, an orange-red gel-like product. These freeze-dried CDs were then used for study.

2.3. Synthesis of 813-CD-25K PEI

The 813-CDs were obtained by means of microwave pyrolysis of IR813 (0.100 g) and PEI MW 25K (0.050 g). The methodology for the synthesis of 813-CD-25K is the same as in Section 2.2. Post pyrolysis, it was observed that no solution remained, leaving a dark black-orange 813-CD (Figure S2B). The product was then purified by flash chromatography with the same eluent system as 813-CD-600 PEI, producing a dark green-orange product labeled 813-CD-25K PEI. These freeze-dried 813-CD-25K PEI CDs were also used in our study.

2.4. Synthesis of 813-CD-600 PEI/PVP Nanocomposite Thin Film

To synthesis 813-CD-600 PEI/PVP nanocomposite thin films, 500 mg of PVP were dissolved in 5 mL of ethanol and sonicated for 1 min. Next, 5.00 mg of 813-CD were also dispersed in 5 mL of ethanol and sonicated for 1 min. The now dispersed solution of 813-CDs was aliquoted into the prepared PVP ethanol solution at 1 mL intervals and was uniformly dispersed under stirring. The obtained mixture was poured into a glass Petri plate and dried for 24 h under ambient conditions in the dark to obtain the 813-CD/PVP film.

2.5. Characterization

UV-vis spectra were obtained from an Agilent Cary 100 UV-vis spectrophotometer. Photoluminescence (PL) characterization was performed on a Fluorolog HORIBA Jobin Yvon fluorometer with a slit width of 5 nm for excitation and emission. All optical charac-

4 of 18 Molecules 2023, 28, 1755

> terization spectra were obtained with quartz cells possessing an optical pathlength of 1 cm. Fourier-transform infrared (FTIR) spectroscopy data were obtained with a PerkinElmer FTIR (Frontier) spectrometer (Waltham, MA, USA) by using the attenuated total reflection (ATR) technique with air as background. The AFM images of 813-CDs were obtained with an Agilent 5420 atomic force microscope (Santa Clara, CA, USA) by using tapping mode. To perform AFM measurements, a drop of diluted 813-CDs aqueous solution was applied on a clean silica mica slide and air dried, which was then transferred to perform the screening using tapping mode. The tip used was silicon (length: 225 μm; thickness: 5 μm) manufactured from Nanosensors with a force constant of 15 N/m. The TEM was performed by using a JEOL 1200 EX TEM (Peabody, MA, USA). For TEM measurements, a drop of the 813-CDs solution was placed on a carbon coated copper grid and air-dried prior to examination. Scanning electron microscopy (SEM) images were taken at 15 KV accelerating voltage on a Hitachi SU1510. The Zeta potential was recorded on a Malvern Zetasizer nano-series. Electrochemical measurements were conducted using a PARSTAT 3000A potentiostat (Ametek Scientific Instruments, Berwyn, PA, USA) as reported in the literature [59].

3. Results and Discussion

3.1. UV-Vis Analysis of 813-CD 600 PEI

The detailed preparation of 813-CDs was described in Section 2. The UV-vis spectroscopy is a suitable tool to assess the electronic structure of conjugated systems. As expected, the absorption spectra of 813-CDs exhibited the typical absorption bands attributed to the π - π * transitions of the C=C bond and the n- π * transition of the C=O bond at 210 and 290 nm, respectively (Figure 1) [60,61]. A band at 375 was found to be similar to that of IR-813, which derives from the $n-\pi^*$ transition of C=N functionalities present in the cyclic systems. Additionally, further bands were found at 450, 545, 590, 665, and 745 nm, respectively. These ranges are hypothesized to be due to the degradation

Molecules 2023, 28, x FOR PEER REVIEW the cyclic structure of IR-813 to form new nitrogen-containing heterocyclic structure of IR-813 to form new nitrogen-contai coordinated with PEI to form new emissive states [62–65]. However, the loss of conjugation is what leads to bands with a hypsochromic shift.

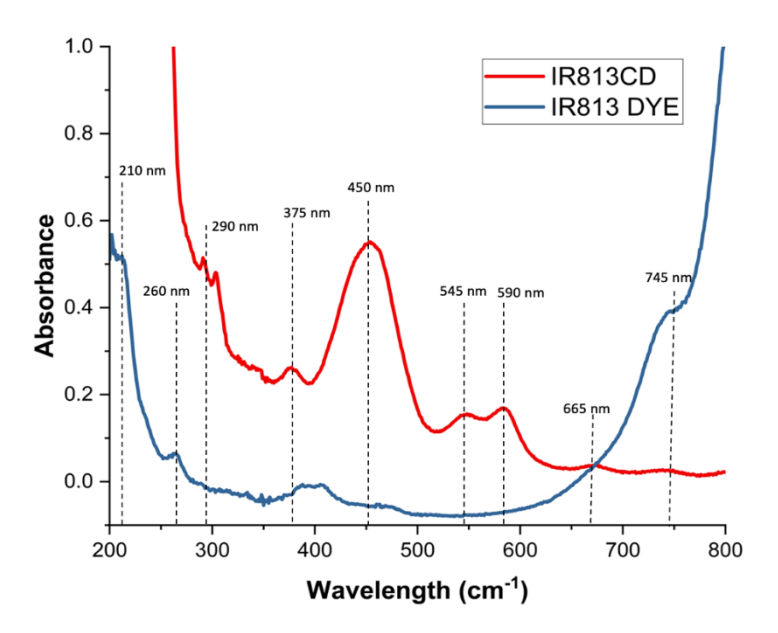


Figure 1. UV-vis analysis of \$13-CDs and IR-\$13 dye.

2. Solvatochromic PL Behavior of 813-CD Solvatochromic PL Behavior of 813-CD Fluorescence spectroscopy is both an ideal and sensitive technique to supplement data fron Turescence apectroscopic in both septicles and sensitive technique to sunglemente data from PUV-vis and understand the fluoressent he baxios of materials that absorb disable The farthest PL peak and its respective PL intensity in counts per second (CPS) of 813-CD-600 PEI (0.1 mg/mL) was recorded to assess the viability of the material in solvent polarity sensing techniques across a wide range of excitation in decreasing solvent polarities in Table 1 (water, ethanol, acetic acid, DMSO, DMF, methylene chloride, chloroform, ethyl acetate, toluene, ether, and hexane, respectively). The expected result was to produce CDs

Molecules **2023**, 28, 1755 5 of 18

PEI (0.1 mg/mL) was recorded to assess the viability of the material in solvent polarity sensing techniques across a wide range of excitation in decreasing solvent polarities in Table 1 (water, ethanol, acetic acid, DMSO, DMF, methylene chloride, chloroform, ethyl acetate, toluene, ether, and hexane, respectively). The expected result was to produce CDs that retained optical properties similar to IR-813, which has notable emission peaks at 600 and 827 nm, respectively. We hypothesized that there may be degradation of the dye during the synthetic process, resulting in slight loss of conjugation. It is this decrease in conjugation that contributes to an increase of the energy band gap, producing a hypsochromic shift. Interestingly, this behavior was observed when the PL of the 813-CDs were excited between 380 to 600 nm, at 20 nm intervals in comparison to IR-813 (Figures S3 and S4). To our surprise, the most polar solvent (water) 813-CDs were found to possess far-red emission at 698 with a PL intensity of 1.5×10^6 (CPS). Interestingly, 813-CDs were found to have a clear isosbestic point at 575 nm. This finding is important because it means that there will be no change in the optical property at a set wavelength and hence, a uniformity in optical properties across the size distribution of CDs. This agrees with our prior hypothesis regarding the emissive origin of our CDs. As the 813-CDs were introduced to environments of decreasing solvent polarity, we started to observe negative solvatochromism. In ethanol, a hypsochromic shift was immediately observed as the farthest emissive peak was found at 650 nm with a PL intensity of 1.4×10^6 (CPS). The same trend occurred as the 813-CDs were exposed to environments with even lower solvent polarity. In acetic acid, the PL shifted to 655 nm with a slight increase of PL intensity $(1.9 \times 10^6 \text{ (CPS)})$. The DMSO possessed PL at 610 nm and had a quite drastic decrease of PL intensity of 5.0×10^5 (CPS). Serving as the midway point of decreasing polarity, both DMF and methylene chloride produced the familiar PL peak at 655, but had a noticeable decrease of PL intensity to 1.1×10^6 and 1.0×10^6 (CPS), respectively. In chloroform, the 813-CDs emitted at 653 nm, but drastically dropped in PL intensity to 2.5×10^5 (CPS). Following the same trend, ethyl acetate, ether, and toluene had observed PL shifts to 650 nm followed by low PL intensities of 8.0×10^5 , 7.2×10^5 , and 3.8×10^5 (CPS), respectively. Notably, in hexane (the lowest polarity), the farthest emissive peak was found to be at 590 nm, meanwhile having the low PL intensity of 4.5×10^5 (CPS).

Table 1. Optical data of 813-CDs (farthest PL and intensity) and solvents used with their respective polarity index.

OPTICAL ANALYSIS OF 813 CDS IN VARIOUS SOLVENTS OF DECREASING POLARITY			
SOLVENT	Polarity Index (P)	Farthest PL (nm)	PL Intensity (CPS)
WATER	1.00	698	$1.5 * 10^6$
ETHANOL	0.654	650	$1.4 * 10^6$
ACETIC ACID	0.648	655	$1.9 * 10^6$
DMSO	0.444	610	$5.0 * 10^5$
DMF	0.386	655	$1.1 * 10^6$
METHYLENE CHLORIDE	0.309	655	$1.0 * 10^6$
CHLOROFORM	0.259	653	$2.5 * 10^5$
ETHYL ACETATE	0.228	650	$8.0*10^{5}$
ETHER	0.117	650	$7.2 * 10^5$
TOLUENE	0.099	650	$3.8 * 10^5$
HEXANE	0.009	590	$4.5 * 10^5$

To address the decrease in PL intensity with decreasing solvent polarity, we hypothesized that in more polar solvents there is the presence of aggregation induced emission (AIE) by particles. This phenomenon leads to more intense emissions at aggregated states in comparison to conventional aggregation fluorescence quenching mechanisms displayed by CDs [66]. From the results of the fluorescence study in various solvents, we propose a schematic illustration of the emission mechanism from 813-CDs in solvents of decreasing polarity (Figure 2). We hypothesized that behavior of the excited-state of 813-CDs is

Molecules **2023**, 28, 1755 6 of 18

dictated by the solute-solvent interactions of various polarities. Specifically, under excitation the solvent molecules have the opportunity to rotationally reorient to stabilize the excited-state dipole moment. This phenomenon as depicted is known as solvent relaxation, which is a key feature of both positive and negative solvatochromism [67–69]. Under this condition, we believe that 813-CDs experience a lowering of the energy of their excited state. Post-emission, the excited 813-CD returns to ground state. According to the literature, as the emission of CDs are linked to their $\pi \to \pi^*$ transition, the polarity of the solvent used will result in a reduction of energy of the first excited state (S₁) than that of the ground state (S₀). Effectively, as solvent polarity increases, the energy gaps between S₀ and S₁ are reduced resulting in longer emitted wavelengths. This phenomenon is attributed to the behavior of more polar solvents to enhance the electron cloud density of the CD's sp² domain which modulates the $\pi \to \pi^*$ electron transition [70]. We also observed the state of the 813-CDs. We hypothesized that this character-

Molecules 2023, 28 presente the throughle-peaked nature of the 813-CDs. We hypothesized that this characteristic is due to a mix of the carbon core state (600 nm) and surface defects from PEI on the surface (697 nm). This is attributed to the transition of a higher singlet electronic state (S₂) undergoing internal conversion to a lower singlet electron state S₁ before returning to S₂. As we observed the drastic red-shifts of 813-CD-25K PEI, the idea of emissive states due to of emissive states due to surface defects made sense as the double-band peak was not consistent in comparison to 813-CD-600 PEI having red shifts as far as 7/6 nm [72]

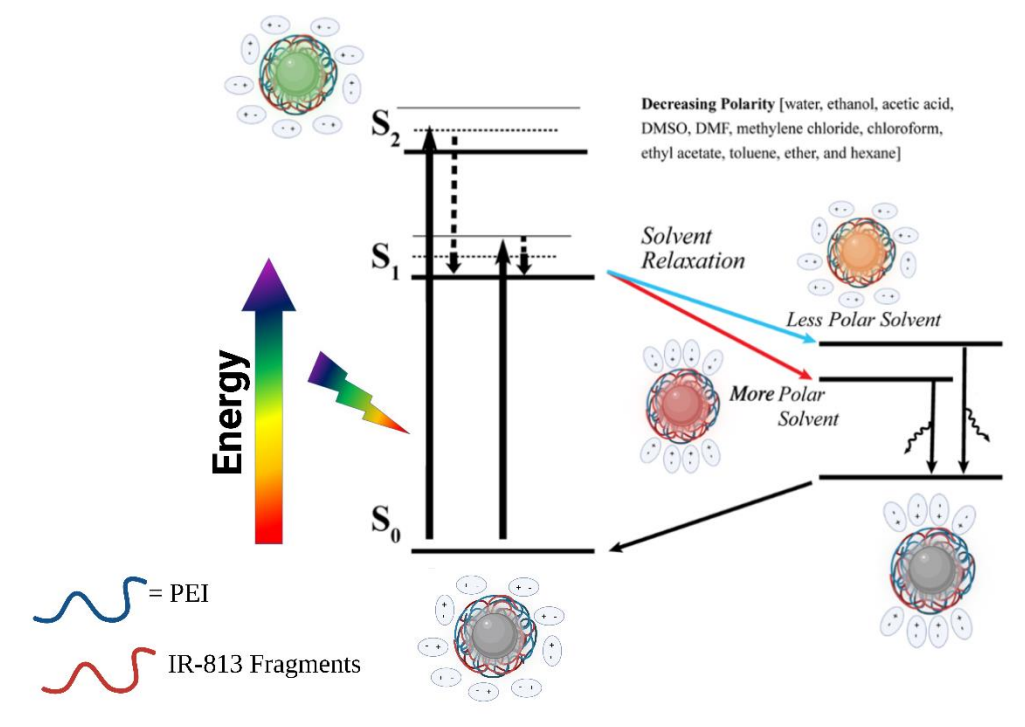


Figure 2. Schematic illustration of the emission mechanism from 813-CDs in solvents of decreasing polarity. Created Fight Bi2/Rendernation lhost stidion of Ellenumiss 2023 mechanism from 813-CDs in solvents of de polarity. Created with BioRender.com, accessed on 1 January 2023.

3.3. Optical Manipulation of 813CDs: 600 PEI vs. 25K PEI

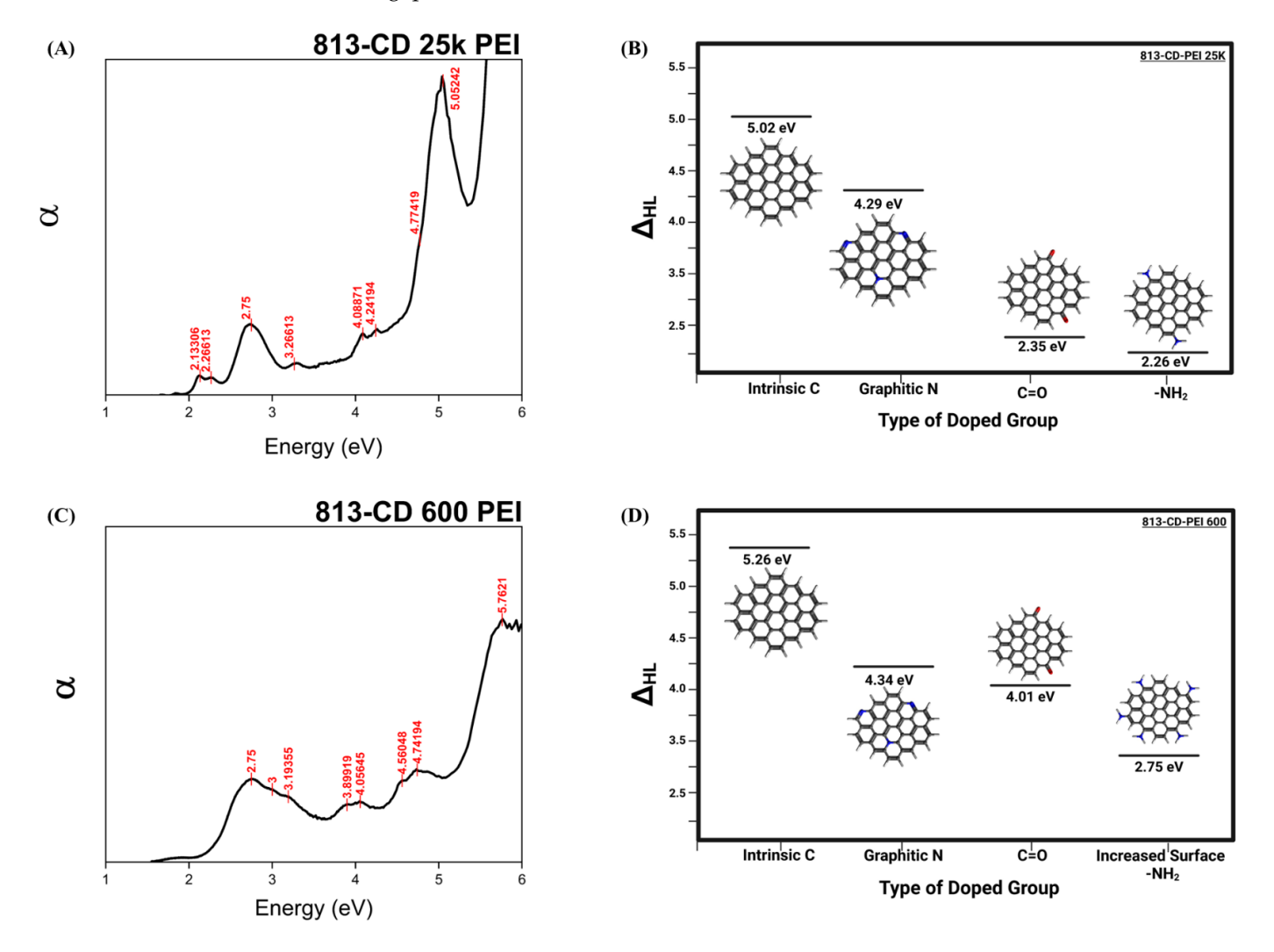
To understand the interpretation of the 813-CDs, α vs energy problem and the properties of the 813-CDs, α vs energy problem and the properties of the insight into the electronic transitions between the political problem as previously described, CD reveal flavorable via UV-vis spectra, the electronic data used in Figure \$5.4 B. An analysis of \$13-CD 25 King the PEI revealed that there every provided in Figure \$5.4 B. An analysis of \$13-CD 25 King the PEI revealed that there every gap (AHI) are provided in Figure \$5.4 B. An analysis of \$13-CD 25 King the PEI revealed that there every gap (AHI) are provided in Figure \$5.4 B. An analysis of \$13-CD 25 King the PEI revealed that there every gap (AHI) are provided in Figure \$5.4 B. An analysis of \$13-CD 25 King the PEI revealed that there every form the provided in Figure \$5.4 B. An analysis of \$13-CD 25 King the PEI revealed that there every form the provided in Figure \$5.4 B. An analysis of \$13-CD 25 King the PEI revealed that there every four final electronic transitions (Figure 3.4 B.) HOMO-We propose that these electronic transitions are due to the type of doped group, such as intrinsic carbon, graphitic nitrogen, carbonyl, and increased surface amines present, respectively (Figure 3.4 B.) Propose that these electronic transitions are due to the type of doped group, such as intrinsic carbon, graphitic nitrogen, carbonyl, and increased surface amines present, respectively (Figure 3.4 B.) Propose that these electronic transitions are due to the type of doped group, such as intrinsic carbon, graphitic nitrogen, carbonyl and increased surface amines present, respectively (Figure 3.4 B.) Propose that these electronic transitions are due to the type of doped group, such as intrinsic carbon, graphitic nitrogen, carbonyl and increased surface amines present, respectively (Figure 3.4 B.)

trinsic carbon, graphitic nitrogen, carbonyl, and increased surface amines present, tively. Our premise is that the increased amount of surface defects from the orient nitrogen-based cyclic structures and amines on the surface of the CDs results in the ering of the energy band gap; thus, causing the emission to be red shifted as the shift range changes. To validate our hypothesis, 813-CD 600 PEI was then screene

Molecules 2023, 28, 1755 7 of 18

> tively. Our premise is that the increased amount of surface defects from the orientation of nitrogen-based cyclic structures and amines on the surface of the CDs results in the lowering of the energy band gap; thus, causing the emission to be red shifted as the stokes shift range changes. To validate our hypothesis, 813-CD 600 PEI was then screened as the material of choice for α vs energy plot for determination as there was less nitrogen present in the same reaction conditions. Therefore, we expected that the band gaps overall would increase slightly. As expected, the analysis of 813-CD 600 PEI revealed that there were four electronic transitions between the HOMO-LUMO states of the CD that resembled that of the prior α vs energy plot. Only the Δ_{HL} was slightly larger, providing Eg values of 5.26, 4.34, 4.01, and 2.75 eV, respectively (Figure 3C,D). This observation made sense as even though there were the same type of doped groups present (intrinsic carbon, graphitic

Molecules 2023, 28, x FOR PEER REVIEWnitrogen, carbonyl, and surface amines present, respectively), with the lowering of http://en content, there were fewer surface defects state present which would lead to a higher energy band gap.



do skup gdosip up 21 5 25k 27k PEL dGz chur gy grosy of 91 xCD 300 PEN (DEM (De Models expression taof this deligible of the deligible d ReiBioRentheraconssectors ad anuly probably 2023.

Substrantial interil preparation between battrast 33CD25KPEI and 813-CD 600 PEI in in water were studied to reveal how the All correlates to the difference capabilities. An Arrbsservation of the Phispsettum of 813-500 25k Perposulates that the lowered and sap gap as eteremined by the asercity plot leads to the fareted mission at 1229 militigate 4. 4A). A second emissive peak was also observed at 600 nm, which decreased in intensity as the excitation wavelength was swept from 400 to 780 nm in 20 nm intervals, respectively. Interestingly, 813-CD 25K PEI was found to exhibit excitation dependence which is common with CDs that contain increased surface defects. Additionally, the normalized

Molecules 2023, 28, 1755 8 of 18

> A second emissive peak was also observed at 600 nm, which decreased in intensity as the excitation wavelength was swept from 400 to 780 nm in 20 nm intervals, respectively. Interestingly, 813-CD 25K PEI was found to exhibit excitation dependence which is common with CDs that contain increased surface defects. Additionally, the normalized PL spectrum revealed that as the excitation wavelength is increased, the far-red emissive peak is further red shifted as far as 776 nm (Figure 4B). As expected, the PL spectrum of 813-CD 600 PEI was quite different regarding its far-red peak which was observed at 697 nm (Figure 4C). This result was expected in correlation to the α vs energy plot which suggests that the Δ_{HL} is at a higher value. At lower excitation wavelengths, 813-CD 600 PEI exhibited excitation dependence with rising emissive peaks at 600, 557, 510, and 445 nm, respectively. (Figure 4D). We posited that during synthesis, the smaller chained PEI formed a variety of

Molecules 2023, 28, x FOR PEER REV heterocyclic structures at the surface of the CD which led to the PL behavior as described.

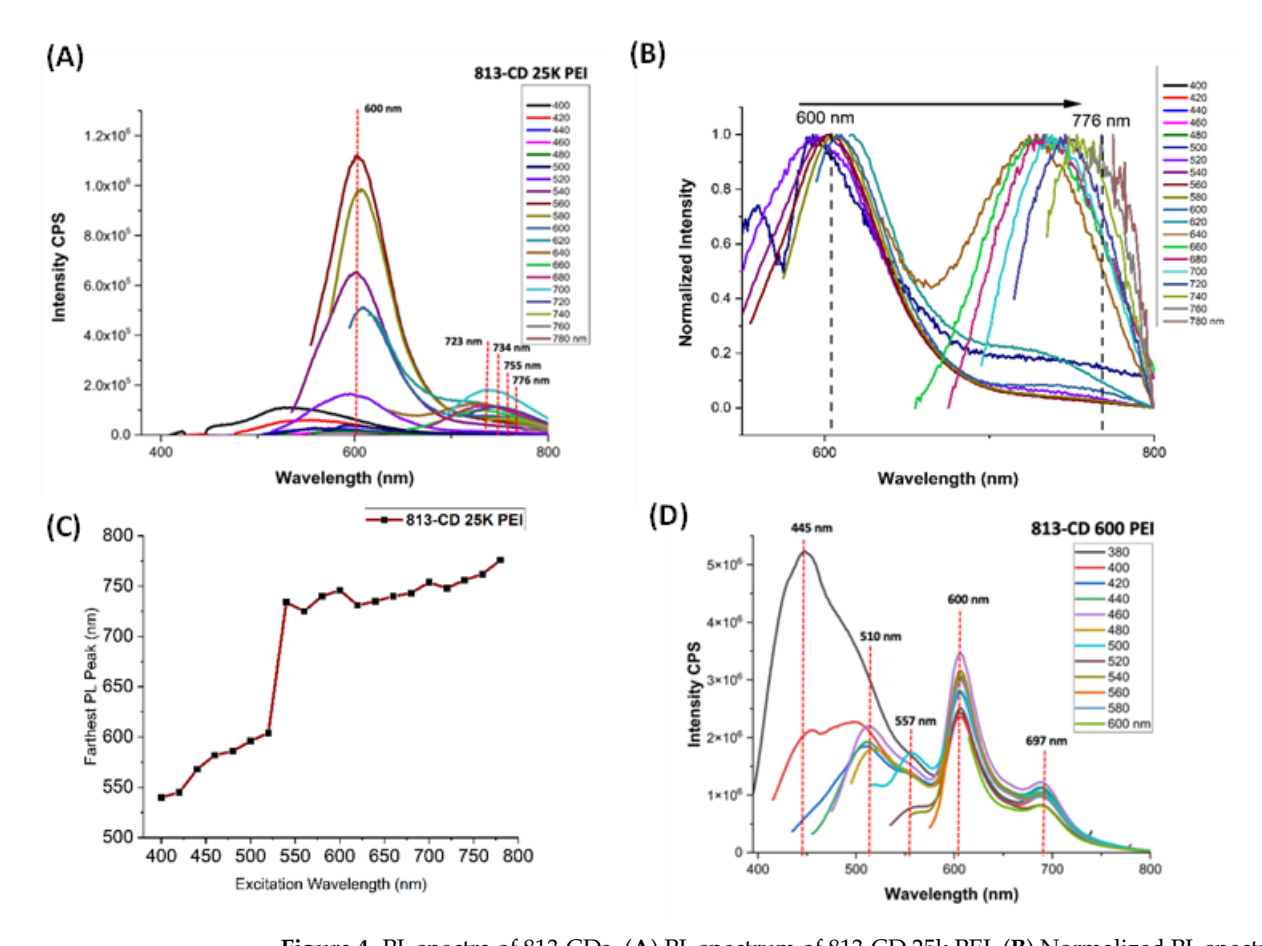


Figure 4. PL spectra of 813-CPs. (A) PL spectrum of 813-CP32s RFIe(B) B) Rimalized Prespectrum of 813CDC35k2BRIPEG) (Corrottos arconel Blappek fon 813rGD32E16 DEK perxeitation avant knasth (ngu). (D)nP.I(D) extrupe cut-8123-6119169 CDE 100 PEI.

There are quite a few perspectives on what factors serve as the emissive origin of GDs &bs:easone asone towards tactor a thot are outside the colon of a vortum confusioner, that associate the emissive shifts of well-defined nanoparticles according to size. The structure property relationship of carbon dots is vague, leading to challenges in elucidating the source of emission. In fact, there are three models currently debated as plausible mechanisms for emission in CDs, i.e., carbon core states, surface states, and molecular thuorescence. Neither mechanisms for emission in CDs, i.e., carbon core states, surface states, and molecular are well defined due to the diversity (size distribution) of CDs which cannot be isolated fluorescence. Neither are well defined due to the diversity (size distribution) of CDs which into just one unitorm product. The CDs are a heterogenous distribution of different-sized cannot be isolated into just one uniform product. The CDs are a heterogenous distribution particles that have the same emissive peak, loosely displaying the quantum size effec of different-sized particles that have the same emissive peak, loosely displaying the a mix of both carbon core and surface states of ca thought stems from a mix of both carbon core and of carbon dots. We posited that 813-CD-600 PEI may have more sp² domain sizes core state behavior) which correlates to the slight size increase, though does not particularly contribute towards red emission [73]. This idea is corroborated by 813-CD-25k PEI which boasts farther red emission, yet has a smaller, more uniform size distribution. Hence, we hypothesized that the CD's emission may be linked to surface defects states of

Molecules **2023**, 28, 1755 9 of 18

which correlates to the slight size increase, though does not particularly contribute towards red emission [72]. This idea is corroborated by 813-CD-25k PEI which boasts farther red emission, yet has a smaller, more uniform size distribution. Hence, we hypothesized that the CD's emission may be linked to surface defects states of the CDs due to the protection of PEI of IR-813 [73].

The FTIR serves as a powerful tool to qualitatively analyze both the core and the functional groups that passivate the surface of CDs, which typically contain oxygen and nitrogen functional groups. A comparative analysis of 813-CDs and the starting material was performed to reveal insight into the surface of the CD (Figure 5). At first glance, both of 20

813-CD 600 and 25K PEI have similar peaks. Upon analysis of 813-CDs, the intense peaks at 1335–1372 cm⁻¹ and 1030–1070 cm⁻¹ are due to the asymmetric S=O and sulfoxide stretching vibrations, respective alternative the same triple is have the sound respective sulfoxide moie trees present from the trees of the stretching of the same tespective peaks. These from the first of the stretching of the same tespective peaks. These from the first of the stretching of the same tespective peaks at 133-CDs retain most functionality from IR-813. A range between the surface peaks at 3480 cm⁻¹ is attributed to the C-H stretching of the sp² carbon species, which 3000–3100 cm⁻¹ fractional complete to the composition of the sp² carbon species, which make attributed to stretching vibrations of 0-H (trace water) present, as well as the medium up the carbonized approach to the complete the stretching of the sp² carbon species, which make attributed to stretching vibrations of 0-H (trace water) present, as well as the medium up the carbonized approach of the stretching to the present at 2850–3000 cm⁻¹ indicative of the stretching to the present at 2850–3000 cm⁻¹ indicative of the special properties of the surface of indicative of the stretching of the same strength of the surface of indicative of the stretching of the same strength of the surface of indicative of the stretching to the surface of the surface of indicative of the surface of the surface of indicative of the surface of the

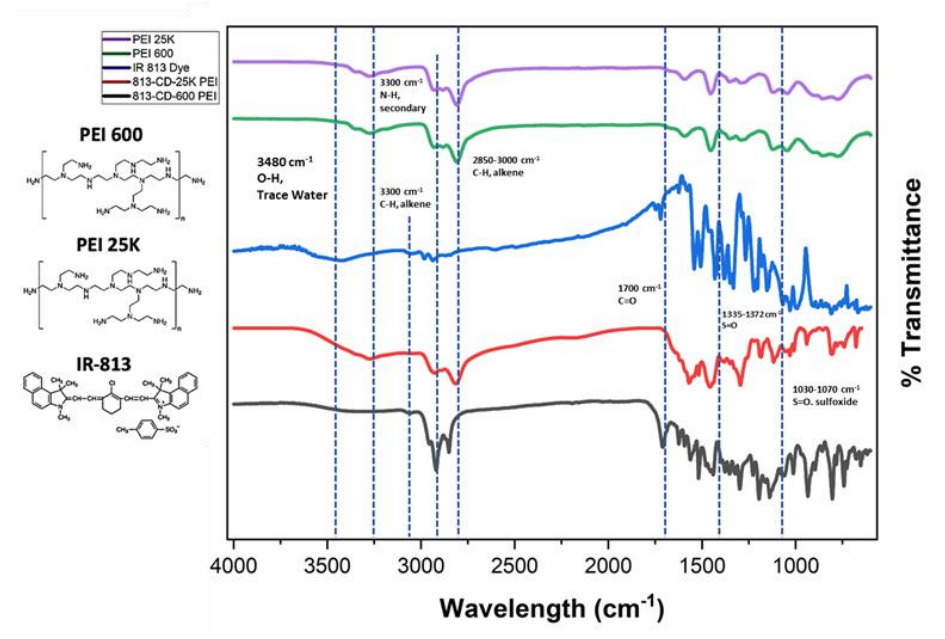


Figure 5. FTIR officient spectrooffs PFI 25K are 1800 years 33 years 1800 years 33 years 1800 years

Functional mainties out two drives of CDs can do sidentified and durantified fly Inches of preprecursors. In general, the discretion of the precursors. In general, the discretion of the precursors of the precursors of the precursors of the precursors of the precursor of t

decomposition steps: 40–376, and 376–673 °C; (4) the CDs (CD-PEI 600) possess four decomposition periods: 40–127, 127–248, 248–463, and 463–673 °C; (5) the CDs (CD-PEI 25K) possess four decomposition periods: 40–200, 200–376, 376–463, and 463–673 °C; (6) both the DTG of PEG 600 and 25K generally show two decomposition stages, but different ranges indicate the effect of molecular weight on the thermostability of polymers; and (7)

(2) PEI 600 has two decomposition steps: 40–463, and 463–673 °C; (3) PEI 25K has two decomposition steps: 40–376, and 376–673 °C; (4) the CDs (CD-PEI 600) possess four decomposition steps: 40–407, 127, 127, 248, 248, 462, cr. l. 462, 673 °C, (5) the CDs (CD PEI 25K)

Molecules 2023, 28, x FOR PEER REVIEWIN position periods: 40–127, 127–248, 248–463, and 463–673 °C; (5) the CDs (CD-PEI 25K)

possess four decomposition periods: 40-200, 200-376, 376-463, and 463-673 $^{\circ}$ C; (6) both the DTG of PEG 600 and 25K generally show two decomposition stages, but different ranges indicate the effect of molecular weight on the thermostability of polymers; and (7) with the with the DTG of a well-established CD species as reference, any peaks between 40–127 °C DTG of a well-established CD species as reference, any peaks between 40–127 °C indicate indicate the loss of water molecules adsorbed on CDs. The mass loss at 127–200 °C suggests the loss of water molecules adsorbed on CDs. The mass loss at 127–200 °C suggests the loss of water molecules generated through intramolecular dehydration condensors of water molecules g sation reactions. The stage between 200–248 °C is attributed to the decomposition of edge-actions. The stage between 200–248 °C is attributed to the decomposition of edge-plane plane oxygen-containing functional groups. The stage at 248–376 °C is due to the decomposition persition of relatively stable oxygen-containing functional decouns and sublimation of small carbón framskygrks. The stage & 1376-463 °C indicates the decomposition of aminary, The stage of the indicates the thres also the notored during sportage CDR (813-per 600) showed become description of maistyre respectively in the ddities and the corresponding AGA Sigues was mass less was absurved among all the other many lex protect are expected due to the price; egycanafingrizzs200 cycing-1927-200 a.G. ED-19EI 29R explicited P325h extribited Isburd 122/errassleenes, water anology democrate aparticulty if a rand the analytical new terral definition of the control of the con tiencional effentioner entriona. Hammeun ai rechivatra mol cultar de la vicione de manti oncon not Pets dannot on union Ball both in Ethic pariodispity Bell dicanot obey and answer principles. IRSSIB-uthering open IR-1814 watains peoch lorates a trien is try that needed as it beyop bearing it is berehippication considering its biditions plaining that of the peak of the pea show-813 the NATG 200 H2481 3 Chindricence 20the 2488 S Grindricens extra distinct force announced metallicing functional uning the sphores sold yield strong ether production of Figure (6B) n(pb) sitiano (Figure 16B), ti(th) obli arguaticad yn stadi i kions y gferelativialiyn ist globa matiy genl-garot aina d'unaction alla groce y och subject de la company de la co bbsefraedeiwalkthe samples veut ing 1486-374m flesutlithes 248-376m flesutlithes 248-376m flesutlithes pensentages ing I&1818, p2EEJe6000g PEIr251K-8C3) 4PH116600, PARIC261K)-CEI-2EK6000, 400% C5949, P3525 K3016, 400% 59%, 85%;eCW/sJyar(d2)19%) segpentily lima(S2) osebs equantly, duasis g.3576s463c. (Greducitoring 37604690 Citibue obathinde and plositions of osacine end 196 81/253 40 1585 veced 576 9818, -816, PE%60AdBEI R5KRC3D3PEE6000 and C5KPED2FKI 600p antively; RE3 L5Kdries the that typically battineth463s676n26 lovelyebay1697873C/masd litsers 6/73016, 1889s 78cs278f 3012, 1888y7246, the preference of the continuous aromatic structures.

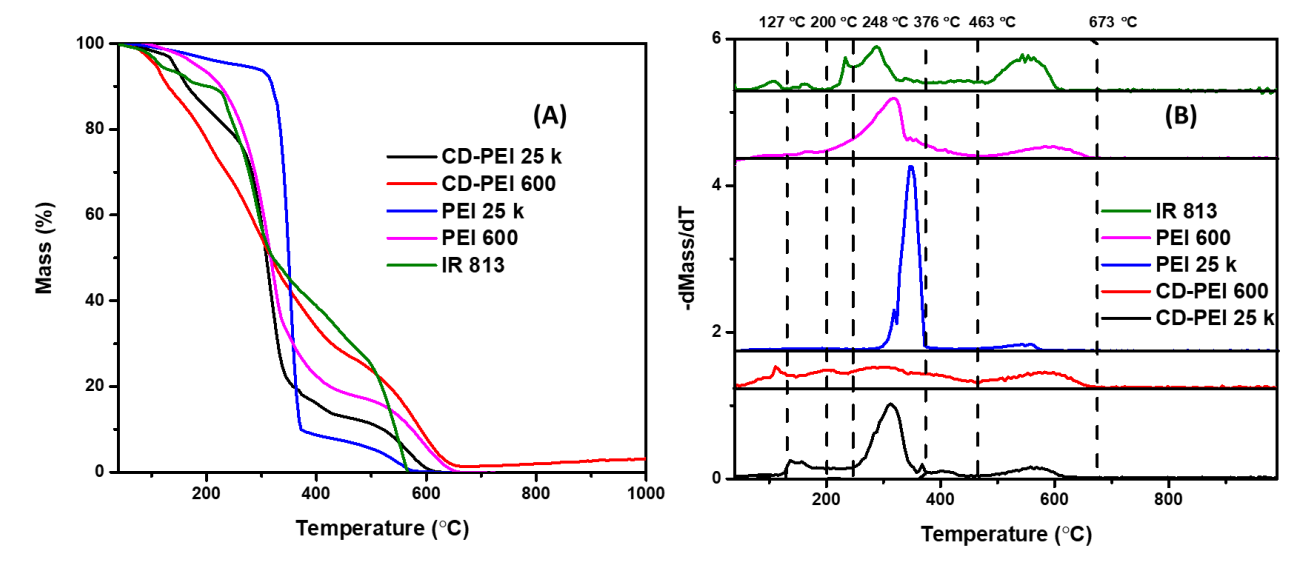


Figure 6. TGA (A) and DTG (B) of CDs and precursors including IR-813, PEI 600 and 25K.

Preliminary consideration of the structure should be based on both TGA and FT-IR data. As shown by TGA data, the aromatics domains represent a relevant amount of both 813-CDs produced by using both PEI 600 and 25 K, and they are due to native aromatic moieties of carbon dots and piperazine-like structure formed during the degradation of PEI [75]. Additionally, IR analysis shows the signal of sulphate proving the persistence of tosyl residues inside the 813-CDs

Preliminary consideration of the structure should be based on both TGA and FT-IR data. As shown by TGA data, the aromatics domains represent a relevant amount of both Molecules 2023, 28, x FOR PEER REVELS-CDs produced by using both PEI 600 and 25 K, and they are due to native aromatic moieties of carbon dots and piperazine-like structure formed during the degradation of PEI [74]. Additionally, IR analysis shows the signal of sulphate proving the persistence of tosyl residues inside the 813-CDs.

Accordingly, we assumed the simultaneous occurrence of three pathways regarding the evolution of PEI, IR 813 and ossly residuced uting the production of 813 13-603, as pertod in Figure 7.7.

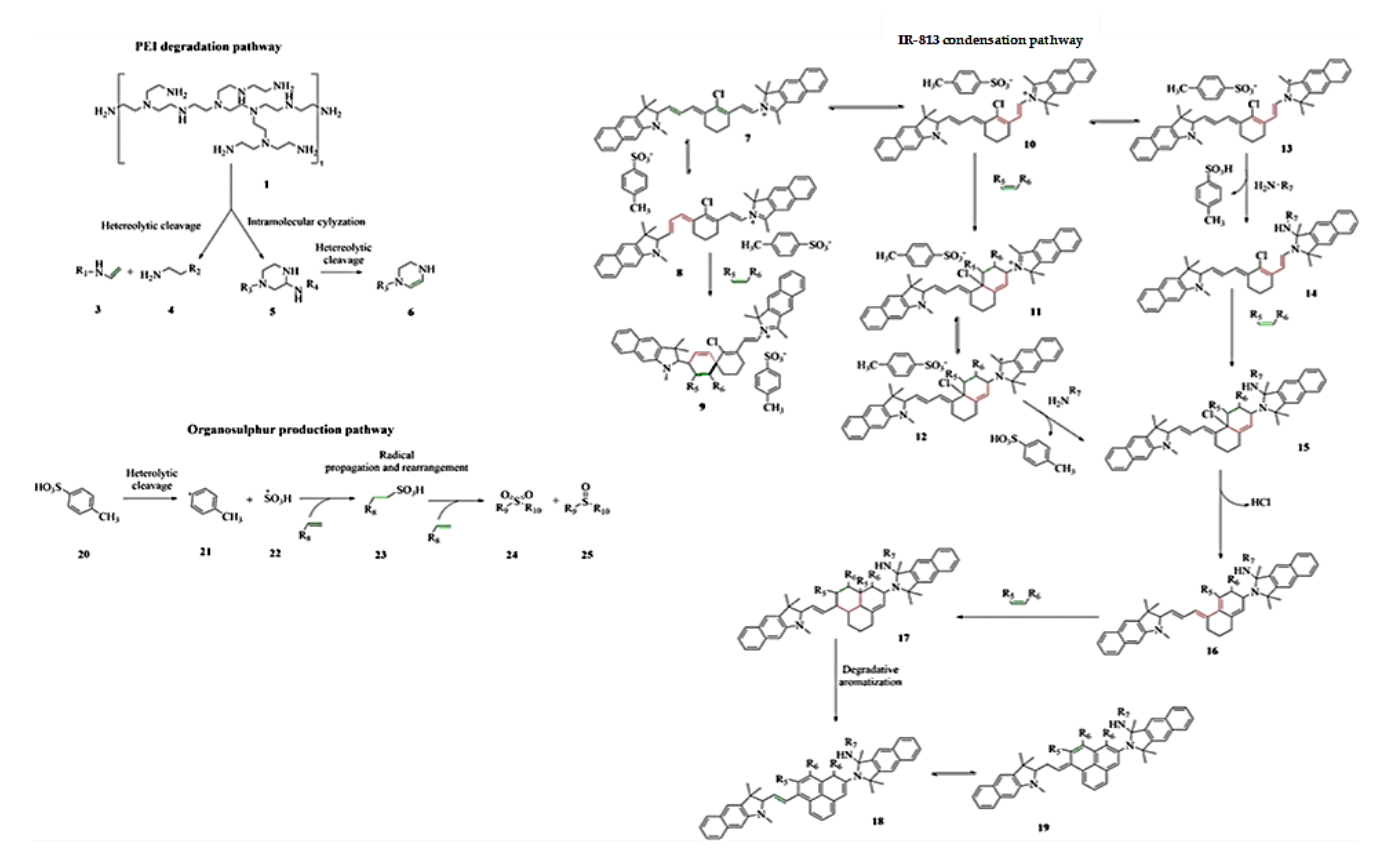


Figure 7. Formation mechanism of \$13-CDs.

The PEI degradation is well described in the literature as reproteby by describe et at 47.5]7.4) it is thorough the tender the control of the literature of the control of the literature of literature of the literature of the literature of the literature of literature of the literature of liter

The equilibrium from 7 to 10 forms cis-diene that could condense producing 12 or reaching the equilibrium with 13. Both 12 and 13 contain a tertiary carbocation that could be a center for mucl opphilic addition of aming supers brooking nacket key an intermediate. 15.13 pie cips cio i could be a rengented diprous that remain a tertiary carbocation that could be a center for mucl opphilic addition of aming supers brooking not a 19 months that presents the formation of the 151-51. The attention of the 151-51. The attention of the 151-51. The attention of the 151-51. The state of the formation of the 151-51. The attention of the 151-51. The 151-51.

The zeta potential of the 813-CD-600 PEI was obtained to further understand both the surface moiety and the surface charge (Table 2). This technique is vital when elucidating the colloidal stability of CDs in various solvents. To preface, an absolute value above 20 mV typically results in CDs that participate in interparticle repulsion [76], effectively producing a well-dispersed colloidal solution. The 813-CD-600 PEI was found to have a

The zeta potential of the 813-CD-600 PEI was obtained to further understand both the surface moiety and the surface charge (Table 2). This technique is vital when elucidating the colloidal stability of CDs in various solvents. To preface, an absolute value above 20 mV typically results in CDs that participate in interparticle repulsion [75], effectively producing a well-dispersed colloidal solution. The 813-CD-600 PEI was found to have a negative potential of -5.11 mV, which suggests that the CDs are composed of negative functional groups such as carboxylic and sulfates on the surface attributed to the functionality left by IR-813 (Figure S6A). Hence, the zeta potential data suggests that the CDs will experience the formation of aggregates in solution, meaning an observation of the aggregates by both the TEM and AFM measurements. A zeta potential analysis of 813-CD 25K PEI revealed a value of +18.8 mV, which corresponds to prior data that postulated that this CD had an increased amount of surface amines that contributed to the positive charge of the material (Figure S6B). Furthermore, the value of the zeta potential suggested that there would be uniformity among the CDs with very little aggregation, as confirmed by both TEM and AFM measurements.

Table 2. Zeta potential of respective 813-CDs.

Carbon Dots	Zeta Potential (mV)	
813-CD-600 PEI	−5.11 mV	
813-CD-25K PEI	+18.8 mV	

The TEM images were studied regarding 813-CDs to understand the X-Y plane size distribution. The sample was sonicated for 15 min prior to measurement to break down any aggregate formation. Analysis indicated that the 813-CD 600 PEI showed a narrow size distribution of 3.0–10.0 nm with a mean size of 5.5 nm (Figure 8A). Additionally, the histogram determined a particle count of over 50 particles with an acceptable degree of uniformity (Figure 8B). The AFM was also performed on the 813-CDs to understand the height profile of the CDs in the z-axis (Figure 8C). The AFM images show that the 813-CD 600 PEI particles are 6–6.5 nm in height, consistent with the previous TEM diameter distribution and confirming the quasi-spherical structure of the 813-CDs. To our surprise, the TEM measurements 813-CD 25K PEI revealed a much smaller and more uniformed narrow size distribution of 2–3.5 nm with a mean size of 2.8 nm (Figure 8D). The histogram of over 500 particles indicates a large degree of uniformity (Figure 8E). These results agree with the AFM measurements which indicate a height profile of roughly 1–2.6 nm (Figure 8F). We propose that the stark difference in size of 813-CD 25K PEI is due to the nature of the larger chained polymer. Specifically, the polymer encases the IR-813 dye during the synthetic process and acts as a barrier to discourage the high degree of carbonization resulting in a smaller particle size, as reported in the literature [76]. In contrast, 813-CD 600 PEI, having a smaller chained polymer, offers less protection; therefore, resulting in a higher degree of carbonization that increases the particle size of the respective CDs.

3.4. Synthesis of 813-CD/PVP Nanocomposite Film

The detailed preparation of 813-CD/PVP nanocomposite thin films were described in Section 2. To assess the solid-state fluorescence of the CDs locked in the PVP polymer matrix, a 535 nm laser was used as a source of excitation onto the 813-CD/PVP film. When light was placed incident onto the face of the thin film, a qualitative bright-orange fluorescence was observed immediately. This phenomenon can be attributed to the absorbance of light by 813-CDs which then emit photons at a longer wavelength, as proposed in Figure 9A. This is in agreement with the literature, which confirms that typical organic fluorophores locked in polymer matrices can attain high optical efficiency due to the spacing of the molecules, discouraging FRET or self-quenching [77–79]. The SEM is a vital tool to elucidate the morphology of the material. As seen in the SEM image (Figure 9B), structural modifications take place in the sample due to interactions of 813-CDs with PVP to produce a surface with

Molecules **2023**, 28, 1755 13 of 18

 $\frac{Molecules 2023, 28, x FOR PEER REVIEW.}{minimal defects}$. The PL of the film produced peaks at both 600 and 650 nm, respectively under 540 nm excitation (Figure 9C).

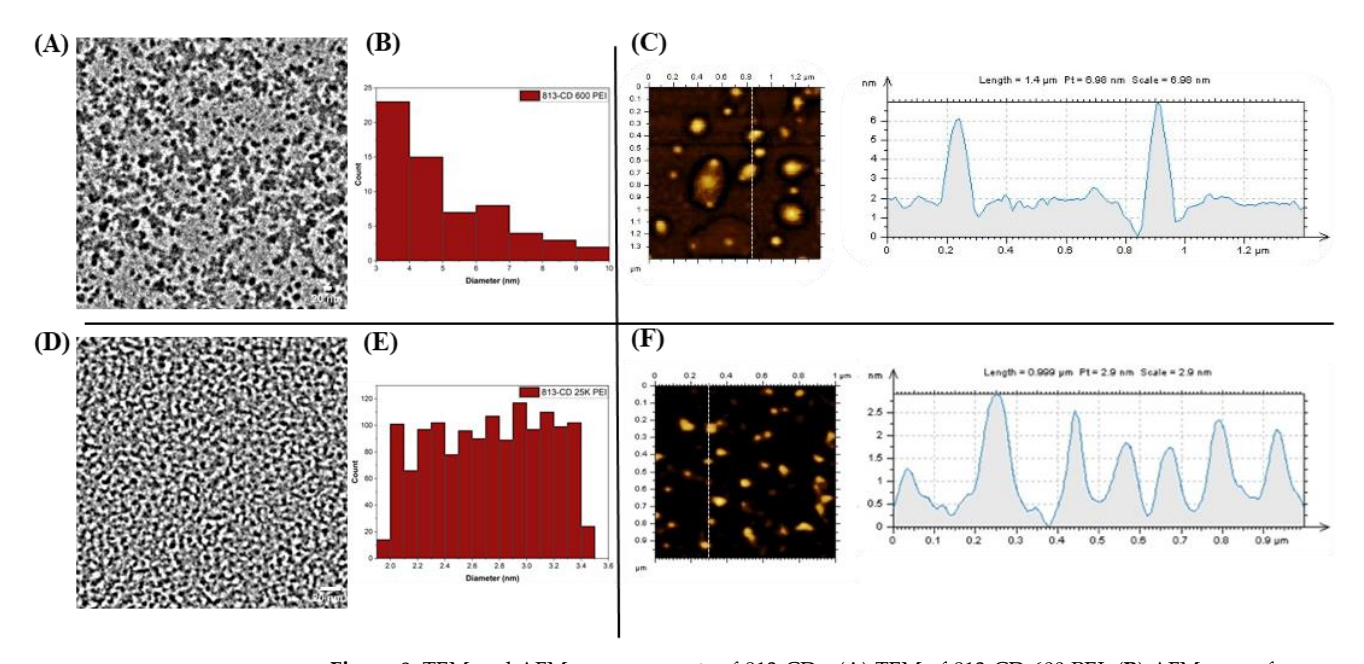


Figure 8. TEM and AFM measurements of 813-CDs. (A) TEM of 813-CD-600 PEL (B) AFM scan of 813-CDs. (B) AFM scan of 813-CDs. (B) AFM scan of 813-CD-600 PEL (B) AFM scan of 813-CD-600 PEL (B) AFM measurements of 813-CD-600 PEL (B) AFM measurements of 813-CD-25K PEL (E) AFM measurements of 813-

of 813-CD-25K PEI. (F) Histogram of 813-CD-25K PEI.

3.4. Synthesis of 813-CD/PVP Nanocomposite Film

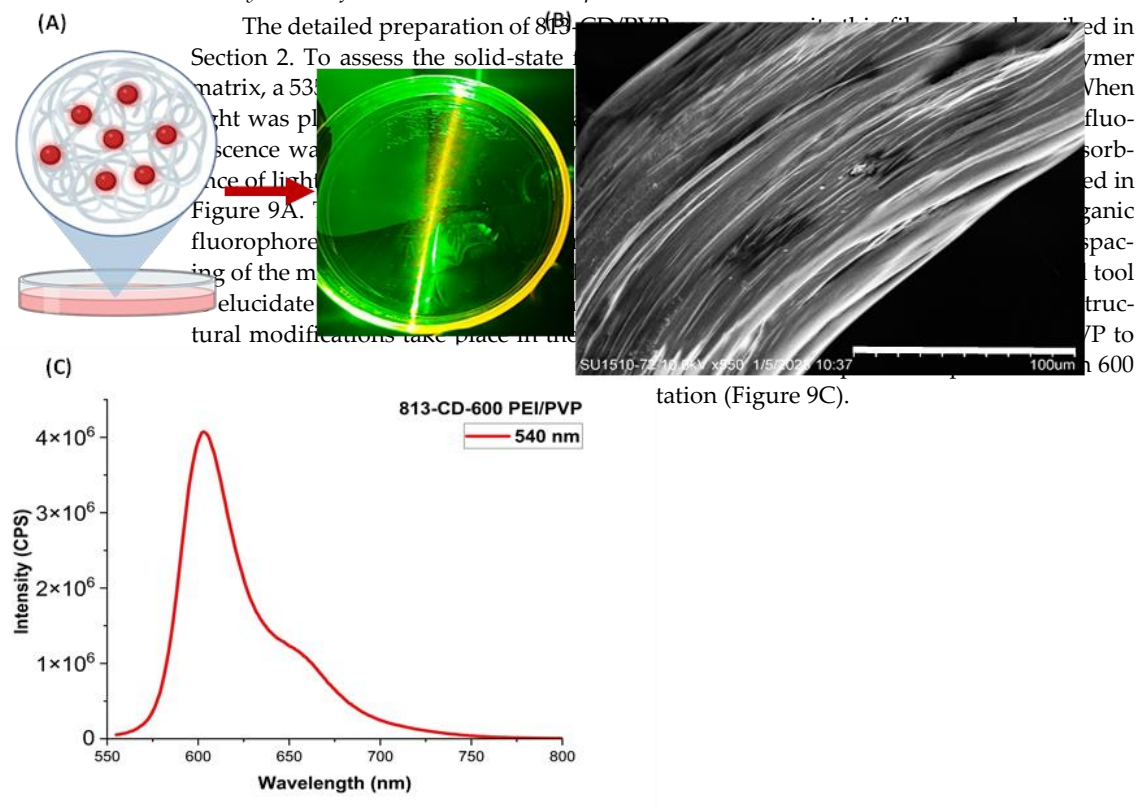


Figure 9. (A) Graphical representation and qualitative assessment of 813-CD/PVP nanocomposite Figure 9. (A) Graphical representation and qualitative assessment of 813-CD/PVP nanocomposite thin films on a glass petricular hunders 33-in the fixelitation activated with Riercond, accessed on 1 January 2023. (B) SEM measurament of 813-CD/PVP huncomposite thin film and 823-CD/PVP nanocomposite thin film and 823

3.5. Cyclic Voltammetry Assessment of 813-CD

The electrochemical behavior of 813-CD as a doping agent for PVP nanocomposites were assessed for applications towards the potential of being used as a coating additive for cathodes to enhance electrochemical performance. In this respect, the literature has shown that PVP film coatings are utilized as additives for a reducing agent to obtain im-

Molecules 2023, 28, 1755 14 of 18

3.5. Cyclic Voltammetry Assessment of 813-CD

The electrochemical behavior of 813-CD as a doping agent for PVP nanocomposites were assessed for applications towards the potential of being used as a coating additive for cathodes to enhance electrochemical performance. In this respect, the literature has shown that PVP film coatings are utilized as additives for a reducing agent to obtain improved stability and rate of lithium ion batteries [80,81]. The presence of these peaks corroborates the n-type nature of our 813-CDs motifs, and are likely a product of the direct reduction of discrete components within the CDs, such as -NH₂ from PEI which coats the surfaces [82–85]. The analyzed system displayed two distinct cathodic peaks at $-0.11 \text{ V} \left(\text{E}_{\text{p}i1} \right)$ and $-0.51 \text{ V} \left(\text{E}_{\text{p}i2} \right)$. These electrochemical signals indicate that the 813-CDs feature two distinct electronic states under electronically reducing conditions (Figure 10A). The respective oxidation peaks were observed at 0.43 V(E_{pi3}) and -0.45 V (E_{pi4}) in the reverse scan sweep. Additionally, the stability of 813-CDs was assessed in cycle scans to understand its usability as an additive for PVP coatings for cathodes. To our surprise, the steady decrease of redox peak intensities was not noticeably significant over time secondary interactions that exist in the system, no major structural reconfiguration occurs

Molecules 2023, 28, x FOR PEER REVIEW 10B). We suggest that due to the increased stability of our 813-CDs and the strong as a function of potential applied, a feature indicative of electrochemical stability [84–86].

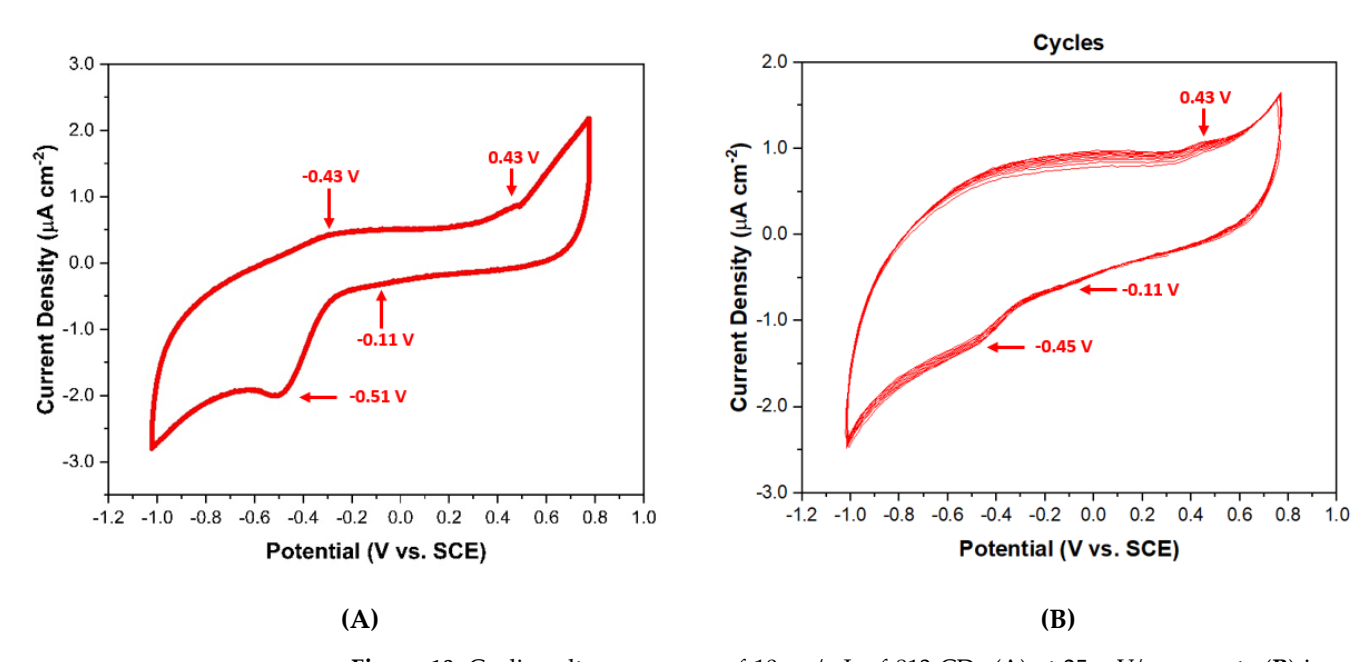


Figure 1.0 Cyrilis william mograms of 10 flys/mil-of 8133 CD2 (A) he 235 my/s sean rate (B) hir espect cycles recorded in H.Ousing ou 1MNaClas supporting electrolyte, glassy carbon (CC) electrode as working electrode, Ag/AgCl as reference electrode, and a Pt wire as a counter electrode. working electrode, Ag/AgCl as reference electrode, and a Pt wire as a counter electrode.

44. Coora blus soons s

FBorthladifist titimae, wed have synthlaoisized chance with poeco freede emititing CIDs that have blee en derived diffrom the reparation of the top of the control of the co is attributed bottletdebre ascrease njuganjog and the of the opploor phone tinsichiet phasipase i thee The long side guides in cistates clarifyed from REInFPELEE, with provee that the this LAD 813 pc Cos applibethphicathent polarity polarity seasing seasingl as well ain a haithpaltrainic thirthin shatem Assummary on the report of the content of the conte Arthiticanilyathinion the finite open to far and amissive CDARISE vector properties that the splint statur differenties allo anission ito the Surpressment of the Selfacille conclusies due to erenterial itsavitab le acca ido ping ingent to ingresse the electror here is althebaxios coll EMR to bepresentially propried by potentially applied as important of cauthor and cottons we halicker that the results of come ter tred emission courses are bighly to variable able property of ⁸V3rGb1e.iTxlevprasepet.istmost3rcmostancermosxensetorixaset imposeesatee axtotingretxwareetto assess the cytotoxicity in cell lines. We are hopeful that once validated, our CDs are to be used as theranostic agents to both image and deliver drugs in vivo with live fluorescence tracking. Recent work from our group involving cationic CDs has shown the capabilities of positively charged CDs to bind with DNA both through electrostatic and intercalative

Molecules **2023**, 28, 1755 15 of 18

lines. We are hopeful that once validated, our CDs are to be used as theranostic agents to both image and deliver drugs in vivo with live fluorescence tracking. Recent work from our group involving cationic CDs has shown the capabilities of positively charged CDs to bind with DNA both through electrostatic and intercalative modes [87]. We hypothesize in this regard that our CDs may be applicable in this field of study in future works.

Supplementary Materials: The following supporting information can be downloaded at: https://www.mdpi.com/article/10.3390/molecules28041755/s1, Figure S1: Graphic illustration of 813-CD synthetic procedure; Figure S2: Images of 813-CDs post-synthesis and purification. (A) Image of 813-CD 600 PEI. (B) Image of 813-CD 25K PEI; Figure S3: PL spectra of 813-CD versus IR-813. (A) PL spectrum of IR-813 from 400–800 nm in methanol. (B) PL spectrum of IR-813 from 750–900 nm in methanol. (C) PL spectrum of 813-CD from 400–800 nm in water; Figure S4: Optical analysis of 813-CDs in various solvents of decreasing polarities according to the solvent polarity index (*P*), PL spectrum. (A) water *P*:1.00, (B) ethanol *P*:0.654, (C) acetic acid *P*:0.648, (D) DMSO *P*:0.444, (E) DMF *P*:0.386, (F) methylene chloride *P*:0.309, (G) chloroform *P*:0.259, (H) ethyl acetate *P*:0.228, (I) ether *P*:0.117, (J) toluene *P*:0.099, and (K) hexane *P*:0.009, respectively. (L) 813-CDs in water under excitation at 535 nm; Figure S5: UV-vis absorbance spectra of 813-CDs in water. (A) UV-vis spectrum of 813-CD 25K PEI from 200–800 nm. (B) UV-vis spectrum of 813-CD 600 PEI from 200–800 nm; Figure S6: Zeta potential of 813-CDs. (A) Zeta potential of 813-CD 600 PEI, -5.11 mV. (B) Zeta potential of 813-CD 25K PEI, +18.8 mV; Table S1: Summary of CD methodology and properties.

Author Contributions: Conceptualization, J.B.D. and R.M.L.; methodology, J.B.D., B.C.L.B.F., Y.Z., W.Z., V.P., J.C., J.B.D. and E.C.; validation, J.B.D. and R.M.L.; formal analysis, J.B.D., B.C.L.B.F., Y.Z., W.Z., Q.J., J.C. and E.C.; investigation, J.B.D., E.C. and R.M.L.; resources, M.B., B.P.S.C., J.-H.O. and A.T.; data curation, J.B.D. and E.C.; writing—original draft preparation, J.B.D.; writing—review and editing, J.B.D., R.M.L., B.C.L.B.F., Y.Z., W.Z., V.P., J.C. and E.C.; visualization, J.B.D. and R.M.L.; supervision, R.M.L.; project administration, R.M.L.; funding acquisition, R.M.L. All authors have read and agreed to the published version of the manuscript.

Funding: This research was supported by the University of Miami with financial support from the National Science Foundation (NSF) grant (1809060 and 2041413).

Institutional Review Board Statement: Not applicable.

Informed Consent Statement: Not applicable.

Data Availability Statement: Not applicable.

Conflicts of Interest: The authors declare no conflict of interest.

References

- 1. Bai, Y.; Zhao, J.; Wang, S.; Lin, T.; Ye, F.; Zhao, S. Carbon Dots with Absorption Red-Shifting for Two-Photon Fluorescence Imaging of Tumor Tissue pH and Synergistic Phototherapy. *ACS Appl. Mater. Interfaces* **2021**, *13*, 35365–35375. [CrossRef]
- 2. Wen, Y.; Jia, Q.; Nan, F.; Zheng, X.; Liu, W.; Wu, J.; Ren, H.; Ge, J.; Wang, P. Pheophytin Derived Near-Infrared-Light Responsive Carbon Dot Assembly as a New Phototheranotic Agent for Bioimaging and Photodynamic Therapy. *Chem. Asian J.* **2019**, *14*, 2162–2168. [CrossRef] [PubMed]
- 3. Sun, S.; Chen, J.; Jiang, K.; Tang, Z.; Wang, Y.; Li, Z.; Liu, C.; Wu, A.; Lin, H. Ce6-Modified Carbon Dots for Multimodal-Imaging-Guided and Single-NIR-Laser-Triggered Photothermal/Photodynamic Synergistic Cancer Therapy by Reduced Irradiation Power. *ACS Appl. Mater. Interfaces* **2019**, *11*, 5791–5803. [CrossRef]
- 4. Du, J.; Xu, N.; Fan, J.; Sun, W.; Peng, X. Carbon Dots for In Vivo Bioimaging and Theranostics. *Small* **2019**, *15*, e1805087. [CrossRef] [PubMed]
- 5. Wang, J.; Zhang, P.; Huang, C.; Liu, G.; Leung, K.C.-F.; Wáng, Y.X.J. High Performance Photoluminescent Carbon Dots for In Vitro and In Vivo Bioimaging: Effect of Nitrogen Doping Ratios. *Langmuir* 2015, *31*, 8063–8073. [CrossRef]
- 6. Yang, S.-T.; Cao, L.; Luo, P.G.; Lu, F.; Wang, X.; Wang, H.; Meziani, M.J.; Liu, Y.; Qi, G.; Sun, Y.-P. Carbon Dots for Optical Imaging In Vivo. *J. Am. Chem. Soc.* **2009**, *131*, 11308–11309. [CrossRef] [PubMed]
- 7. He, C.; Lin, X.; Mei, Y.; Luo, Y.; Yang, M.; Kuang, Y.; Yi, X.; Zeng, W.; Huang, Q.; Zhong, B. Recent Advances in Carbon Dots for In Vitro/Vivo Fluorescent Bioimaging: A Mini-Review. *Front. Chem.* **2022**, *10*, 905475. [CrossRef]
- 8. Ji, C.; Zhou, Y.; Leblanc, R.M.; Peng, Z. Recent Developments of Carbon Dots in Biosensing: A Review. *ACS Sensors* **2020**, *5*, 2724–2741. [CrossRef] [PubMed]

9. Zhou, Y.; Mintz, K.J.; Sharma, S.K.; Leblanc, R.M. Carbon Dots: Diverse Preparation, Application, and Perspective in Surface Chemistry. *Langmuir* **2019**, *35*, 9115–9132. [CrossRef] [PubMed]

- 10. Wu, J.; Chen, G.; Jia, Y.; Ji, C.; Wang, Y.; Zhou, Y.; Leblanc, R.M.; Peng, Z. Carbon dot composites for bioapplications: A review. *J. Mater. Chem. B* **2022**, *10*, 843–869. [CrossRef] [PubMed]
- 11. Peng, Z.; Miyanji, E.H.; Zhou, Y.; Pardo, J.; Hettiarachchi, S.D.; Li, S.; Blackwelder, P.L.; Skromne, I.; Leblanc, R.M. Carbon dots: Promising biomaterials for bone-specific imaging and drug delivery. *Nanoscale* **2017**, *9*, 17533–17543. [CrossRef]
- 12. Gavalas, S.; Kelarakis, A. Towards Red Emissive Systems Based on Carbon Dots. Nanomaterials 2021, 11, 2089. [CrossRef]
- 13. Zhao, M.; Guo, Y.-S.; Xu, W.-N.; Zhao, Y.-F.; Xie, H.-Y.; Li, H.-J.; Chen, X.-F.; Zhao, R.-S.; Guo, D.-S. Far-red to near-infrared fluorescent probes based on silicon-substituted xanthene dyes for sensing and imaging. *TrAC Trends Anal. Chem.* **2020**, 122, 115704. [CrossRef]
- 14. Jun, Y.W.; Kim, H.R.; Reo, Y.J.; Dai, M.; Ahn, K.H. Addressing the autofluorescence issue in deep tissue imaging by two-photon microscopy: The significance of far-red emitting dyes. *Chem. Sci.* **2017**, *8*, 7696–7704. [CrossRef] [PubMed]
- 15. Wang, J.; Zhu, Y.; Wang, L. Synthesis and Applications of Red-Emissive Carbon Dots. *Chem. Rec.* **2019**, 19, 2083–2094. [CrossRef] [PubMed]
- 16. Ge, J.; Jia, Q.; Liu, W.; Guo, L.; Liu, Q.; Lan, M.; Zhang, H.; Meng, X.; Wang, P. Red-Emissive Carbon Dots for Fluorescent, Photoacoustic, and Thermal Theranostics in Living Mice. *Adv. Mater.* **2015**, 27, 4169–4177. [CrossRef] [PubMed]
- 17. Sun, S.; Zhang, L.; Jiang, K.; Wu, A.; Lin, H. Toward High-Efficient Red Emissive Carbon Dots: Facile Preparation, Unique Properties, and Applications as Multifunctional Theranostic Agents. *Chem. Mater.* **2016**, *28*, 8659–8668. [CrossRef]
- 18. Gao, D.; Zhao, H.; Chen, X.; Fan, H. Recent advance in red-emissive carbon dots and their photoluminescent mechanisms. *Mater. Today Chem.* **2018**, *9*, 103–113. [CrossRef]
- 19. Hallaji, Z.; Bagheri, Z.; Kalji, S.-O.; Ermis, E.; Ranjbar, B. Recent advances in the rational synthesis of red-emissive carbon dots for nanomedicine applications: A review. *Flatchem* **2021**, *29*, 100271. [CrossRef]
- 20. Yang, X.; Ai, L.; Yu, J.; Waterhouse, G.I.N.; Sui, L.; Ding, J.; Zhang, B.; Yong, X.; Lu, S. Photoluminescence mechanisms of red-emissive carbon dots derived from non-conjugated molecules. *Sci. Bull.* **2022**, *67*, 1450–1457. [CrossRef]
- 21. Apter, B.; Lapshina, N.; Barhom, H.; Fainberg, B.; Handelman, A.; Accardo, A.; Diaferia, C.; Ginzburg, P.; Morelli, G.; Rosenman, G. Fluorescence Phenomena in Amyloid and Amyloidogenic Bionanostructures. *Crystals* **2020**, *10*, 668. [CrossRef]
- 22. Tauc, J. Optical properties and electronic structure of amorphous Ge and Si. Mater. Res. Bull. 1968, 3, 37-46. [CrossRef]
- 23. Ren, J.; Malfatti, L.; Enzo, S.; Carbonaro, C.M.; Calvillo, L.; Granozzi, G.; Innocenzi, P. Boron oxynitride two-colour fluorescent dots and their incorporation in a hybrid organic-inorganic film. *J. Colloid Interface Sci.* **2020**, *560*, 398–406. [CrossRef]
- 24. Kundelev, E.V.; Tepliakov, N.V.; Leonov, M.Y.; Maslov, V.G.; Baranov, A.V.; Fedorov, A.V.; Rukhlenko, I.D.; Rogach, A.L. Towards Bright Red-Emissive Carbon Dots through Controlling Interaction among Surface Emission Centers. *J. Phys. Chem. Lett.* **2020**, *11*, 8121–8127. [CrossRef]
- 25. Reckmeier, C.J.; Wang, Y.; Zboril, R.; Rogach, A.L. Influence of Doping and Temperature on Solvatochromic Shifts in Optical Spectra of Carbon Dots. *J. Phys. Chem. C* **2016**, *120*, 10591–10604. [CrossRef]
- 26. Alaş, M.; Genç, R. Solvatochromic Surface-Passivated Carbon Dots for Fluorometric Moisture Sensing in Organic Solvents. *ACS Appl. Nano Mater.* **2021**, *4*, 7974–7987. [CrossRef]
- 27. Basu, N.; Mandal, D. Solvatochromic Response of Carbon Dots: Evidence of Solvent Interaction with Different Types of Emission Centers. *J. Phys. Chem. C* **2018**, 122, 18732–18741. [CrossRef]
- 28. Wang, H.; Haydel, P.; Sui, N.; Wang, L.; Liang, Y.; Yu, W.W. Wide emission shifts and high quantum yields of solvatochromic carbon dots with rich pyrrolic nitrogen. *Nano Res.* **2020**, *13*, 2492–2499. [CrossRef]
- 29. Vijeata, A.; Chaudhary, G.R.; Umar, A.; Chaudhary, S. Distinctive Solvatochromic Response of Fluorescent Carbon Dots Derived from Different Components of Aegle Marmelos Plant. *Eng. Sci.* **2021**, *15*, 197–209. [CrossRef]
- 30. Kundu, A.; Park, B.; Oh, J.; Sankar, K.V.; Ray, C.; Kim, W.S.; Jun, S.C. Multicolor emissive carbon dot with solvatochromic behavior across the entire visible spectrum. *Carbon* **2020**, *156*, 110–118. [CrossRef]
- 31. Zhu, X.; Wang, J.; Zhu, Y.; Jiang, H.; Tan, D.; Xu, Z.; Mei, T.; Li, J.; Xue, L.; Wang, X. Green emitting N,S-co-doped carbon dots for sensitive fluorometric determination of Fe(III) and Ag(I) ions, and as a solvatochromic probe. *Microchim. Acta* **2018**, *185*, 510. [CrossRef] [PubMed]
- 32. Arshad, F.; Pal, A.; Rahman, M.A.; Ali, M.; Khan, J.A.; Sk, M.P. Insights on the solvatochromic effects in N-doped yellow-orange emissive carbon dots. *New J. Chem.* **2018**, 42, 19837–19843. [CrossRef]
- 33. Ishchenko, A.A.; Kulinich, A.V.; Bondarev, S.L.; Knyukshto, V.N. Electronic structure and fluorescent properties of malononitrile-based merocyanines with positive and negative solvatochromism. *Opt. Spectrosc.* **2008**, *104*, 57–68. [CrossRef]
- 34. Domínguez, M.; Rezende, M.C. Towards a unified view of the solvatochromism of phenolate betaine dyes. *J. Phys. Org. Chem.* **2010**, 23, 156–170. [CrossRef]
- 35. Ren, J.; Sun, J.; Sun, X.; Song, R.; Xie, Z.; Zhou, S. Precisely Controlled Up/Down-Conversion Liquid and Solid State Photoluminescence of Carbon Dots. *Adv. Opt. Mater.* **2018**, *6*, 1800115. [CrossRef]
- 36. Yoshinaga, T.; Shinoda, M.; Iso, Y.; Isobe, T.; Ogura, A.; Takao, K.-I. Glycothermally Synthesized Carbon Dots with Narrow-Bandwidth and Color-Tunable Solvatochromic Fluorescence for Wide-Color-Gamut Displays. *ACS Omega* **2021**, *6*, 1741–1750. [CrossRef] [PubMed]

Molecules **2023**, 28, 1755 17 of 18

37. Badawi, A. Enhancement of the optical properties of PVP using Zn1-xSnxS for UV-region optical applications. *Appl. Phys. A* **2021**, 127, 1–9. [CrossRef]

- 38. Agool, I.R.; Kadhim, K.J.; Hashim, A. Synthesis of (PVA–PEG–PVP–ZrO2) nanocomposites for energy release and gamma shielding applications. *Int. J. Plast. Technol.* **2017**, 21, 444–453. [CrossRef]
- 39. Carotenuto, G.; Pepe, G.P.; Nicolais, L. Preparation and characterization of nano-sized Ag/PVP composites for optical applications. *Eur. Phys. J. B* **2000**, *16*, 11–17. [CrossRef]
- 40. Husain, M.S.B.; Gupta, A.; Alashwal, B.Y.; Sharma, S. Synthesis of PVA/PVP based hydrogel for biomedical applications: A review. *Energy Sources Part A Recover. Util. Environ. Eff.* **2018**, 40, 2388–2393. [CrossRef]
- 41. Rao, C.V.S.; Ravi, M.; Raja, V.; Bhargav, P.B.; Sharma, A.K.; Rao, V.V.R.N. Preparation and characterization of PVP-based polymer electrolytes for solid-state battery applications. *Iran. Polym. J.* **2012**, *21*, 531–536. [CrossRef]
- 42. Teodorescu, M.; Bercea, M.; Morariu, S. Biomaterials of PVA and PVP in medical and pharmaceutical applications: Perspectives and challenges. *Biotechnol. Adv.* **2019**, *37*, 109–131. [CrossRef] [PubMed]
- 43. Lochhead, R.Y. The Role of Polymers in Cosmetics: Recent Trends. In *Cosmetic Nanotechnology*; ACS Symposium Series; American Chemical Society: Hattiesburg, MS, USA, 2007; Volume 961, pp. 3–56.
- 44. Feng, T.; Zhu, S.; Zeng, Q.; Lu, S.; Tao, S.; Liu, J.; Yang, B. Supramolecular Cross-Link-Regulated Emission and Related Applications in Polymer Carbon Dots. *ACS Appl. Mater. Interfaces* **2018**, *10*, 12262–12277. [CrossRef]
- 45. Yan, F.; Zhang, H.; Xu, J.; Wu, Y.; Zang, Y.; Sun, J. Color Emission Carbon Dots with Quench-ResixAstant Solid-State Fluorescence for Light-Emitting Diodes. *ACS Sustain. Chem. Eng.* **2021**, *9*, 3901–3908. [CrossRef]
- 46. Ren, J.; Stagi, L.; Innocenzi, P. Fluorescent carbon dots in solid-state: From nanostructures to functional devices. *Prog. Solid State Chem.* **2021**, *62*, 100295. [CrossRef]
- 47. Javanbakht, S.; Namazi, H. Solid state photoluminescence thermoplastic starch film containing graphene quantum dots. *Carbohydr. Polym.* 2017, 176, 220–226. [CrossRef] [PubMed]
- 48. Arshad, F.; Pal, A.; Sk, M.P. Review—Aggregation-Induced Emission in Carbon Dots for Potential Applications. *ECS J. Solid State Sci. Technol.* **2021**, *10*, 021001. [CrossRef]
- 49. Li, H.; Su, D.; Gao, H.; Yan, X.; Kong, D.; Jin, R.; Liu, X.; Wang, C.; Lu, G. Design of Red Emissive Carbon Dots: Robust Performance for Analytical Applications in Pesticide Monitoring. *Anal. Chem.* **2020**, *92*, 3198–3205. [CrossRef] [PubMed]
- 50. Havrdova, M.; Hola, K.; Skopalik, J.; Tománková, K.; Petr, M.; Cepe, K.; Polakova, K.; Tucek, J.; Bourlinos, A.B.; Zboril, R. Toxicity of carbon dots-Effect of surface functionalization on the cell viability, reactive oxygen species generation and cell cycle. *Carbon* **2016**, *99*, 238–248. [CrossRef]
- 51. Moghimi, S.M.; Symonds, P.; Murray, J.C.; Hunter, A.C.; Debska, G.; Szewczyk, A.C. A two-stage poly(ethylenimine)-mediated cytotoxicity: Implications for gene transfer/therapy. *Mol. Ther.* **2005**, *11*, 990–995. [CrossRef]
- 52. Iida, T.; Mori, T.; Katayama, Y.; Niidome, T. Overall interaction of cytosolic proteins with the PEI/DNA complex. *J. Control. Release* **2007**, *118*, 364–369. [CrossRef]
- 53. Kircheis, R.; Wightman, L.; Wagner, E. Design and gene delivery activity of modified polyethylenimines. *Adv. Drug Deliv. Rev.* **2001**, 53, 341–358. [CrossRef]
- 54. Wang, C.; Xu, Z.; Zhang, C. Polyethyleneimine-Functionalized Fluorescent Carbon Dots: Water Stability, pH Sensing, and Cellular Imaging. *Chemnanomat* **2015**, *1*, 122–127. [CrossRef]
- 55. Yin, J.-Y.; Liu, H.-J.; Jiang, S.; Chen, Y.; Yao, Y. Hyperbranched Polymer Functionalized Carbon Dots with Multistimuli-Responsive Property. *ACS Macro Lett.* **2013**, 2, 1033–1037. [CrossRef] [PubMed]
- 56. Ashcraft, A.; Liu, K.; Mukhopadhyay, A.; Paulino, V.; Liu, C.; Bernard, B.; Husainy, D.; Phan, T.; Olivier, J.-H.H. A Molecular Strategy to Lock-in the Conformation of a Perylene Bisimide-Derived Supramolecular Polymer. *Angew. Chem. Int. Ed.* **2020**, *59*, 7487–7493. [CrossRef] [PubMed]
- 57. Zhou, Y.; Zahran, E.M.; Quiroga, B.A.; Perez, J.; Mintz, K.J.; Peng, Z.; Liyanage, P.Y.; Pandey, R.R.; Chusuei, C.C.; Leblanc, R.M. Size-dependent photocatalytic activity of carbon dots with surface-state determined photoluminescence. *Appl. Catal. B Environ.* **2019**, 248, 157–166. [CrossRef] [PubMed]
- 58. Hettiarachchi, S.D.; Graham, R.M.; Mintz, K.J.; Zhou, Y.; Vanni, S.; Peng, Z.; Leblanc, R.M. Triple conjugated carbon dots as a nano-drug delivery model for glioblastoma brain tumors. *Nanoscale* **2019**, *11*, 6192–6205. [CrossRef] [PubMed]
- 59. Liu, E.; Li, D.; Zhou, X.; Zhou, G.; Xiao, H.; Zhou, D.; Tian, P.; Guo, R.; Qu, S. Highly Emissive Carbon Dots in Solid State and Their Applications in Light-Emitting Devices and Visible Light Communication. *ACS Sustain. Chem. Eng.* **2019**, 7, 9301–9308. [CrossRef]
- 60. Xu, X.; Cai, L.; Hu, G.; Mo, L.; Zheng, Y.; Hu, C.; Lei, B.; Zhang, X.; Liu, Y.; Zhuang, J. Red-emissive carbon dots from spinach: Characterization and application in visual detection of time. *J. Lumin.* **2020**, 227, 117534. [CrossRef]
- 61. Hu, Y.; Al Awak, M.M.; Yang, F.; Yan, S.; Xiong, Q.; Wang, P.; Tang, Y.; Yang, L.; LeCroy, G.E.; Hou, X.; et al. Photoexcited state properties of carbon dots from thermally induced functionalization of carbon nanoparticles. *J. Mater. Chem. C* **2016**, *4*, 10554–10561. [CrossRef] [PubMed]
- 62. Li, R.; Wei, F.; Wu, X.; Zhou, P.; Chen, Q.; Cen, Y.; Xu, G.; Cheng, X.; Zhang, A.; Hu, Q. PEI modified orange emissive carbon dots with excitation-independent fluorescence emission for cellular imaging and siRNA delivery. *Carbon* **2021**, 177, 403–411. [CrossRef]
- 63. Ru, Y.; Waterhouse, G.I.N.; Lu, S. Aggregation in carbon dots. Aggregate 2022, 3, e296. [CrossRef]

- 64. Nigam, S.; Rutan, S. Principles and Applications of Solvatochromism. Appl. Spectrosc. 2001, 55, 362A–370A. [CrossRef]
- 65. de Melo, C.E.A.; Nandi, L.G.; Domínguez, M.; Rezende, M.C.; Machado, V.G. Solvatochromic behavior of dyes with dimethy-lamino electron-donor and nitro electron-acceptor groups in their molecular structure. *J. Phys. Org. Chem.* **2015**, *28*, 250–260. [CrossRef]
- 66. Reichardt, C. Solvatochromic Dyes as Solvent Polarity Indicators. Chem. Rev. 1994, 94, 2319–2358. [CrossRef]
- 67. Yang, Z.; Li, H.; Xu, T.; She, M.; Chen, J.; Jia, X.; Liu, P.; Liu, X.; Li, J. Red emissive carbon dots as a fluorescent sensor for fast specific monitoring and imaging of polarity in living cells. *J. Mater. Chem. A* **2023**, *11*, 2679–2689. [CrossRef]
- 68. Liu, J.; Li, R.; Yang, B. Carbon Dots: A New Type of Carbon-Based Nanomaterial with Wide Applications. *ACS Cent. Sci.* **2020**, *6*, 2179–2195. [CrossRef] [PubMed]
- 69. Zhu, S.; Song, Y.; Zhao, X.; Shao, J.; Zhang, J.; Yang, B. The photoluminescence mechanism in carbon dots (graphene quantum dots, carbon nanodots, and polymer dots): Current state and future perspective. *Nano Res.* **2015**, *8*, 355–381. [CrossRef]
- 70. Yan, F.; Sun, Z.; Zhang, H.; Sun, X.; Jiang, Y.; Bai, Z. The fluorescence mechanism of carbon dots, and methods for tuning their emission color: A review. *Microchim. Acta* **2019**, *186*, 583. [CrossRef] [PubMed]
- 71. Kosheleva, I.M.; Gembitskii, P.A.; Chmarin, A.I.; Kolesova, L.M.; Zhuk, D.S.; Kargin, V.A. Some properties and the structure of high-molecular polyethylenimine. *Russ. Chem. Bull.* **1971**, *20*, 1536–1541. [CrossRef]
- 72. Zhang, Y.; Yang, M.; Portney, N.G.; Cui, D.; Budak, G.; Ozbay, E.; Ozkan, M.; Ozkan, C.S. Zeta potential: A surface electrical characteristic to probe the interaction of nanoparticles with normal and cancer human breast epithelial cells. *Biomed. Microdevices* **2008**, *10*, 321–328. [CrossRef] [PubMed]
- 73. Xia, C.; Zhu, S.; Feng, T.; Yang, M.; Yang, B. Evolution and Synthesis of Carbon Dots: From Carbon Dots to Carbonized Polymer Dots. *Adv. Sci.* **2019**, *6*, 1901316. [CrossRef] [PubMed]
- 74. Zhang, Y.; Zhuo, P.; Yin, H.; Fan, Y.; Zhang, J.; Liu, X.; Chen, Z. Solid-State Fluorescent Carbon Dots with Aggregation-Induced Yellow Emission for White Light-Emitting Diodes with High Luminous Efficiencies. *ACS Appl. Mater. Interfaces* **2019**, *11*, 24395–24403. [CrossRef]
- 75. Wei, S.; Li, Z.; Lu, W.; Liu, H.; Zhang, J.; Chen, T.; Tang, B.Z. Multicolor Fluorescent Polymeric Hydrogels. *Angew. Chem. Int. Ed.* **2021**, *60*, 8608–8624. [CrossRef]
- 76. Feng, Z.; Adolfsson, K.H.; Xu, Y.; Fang, H.; Hakkarainen, M.; Wu, M. Carbon dot/polymer nanocomposites: From green synthesis to energy, environmental and biomedical applications. *Sustain. Mater. Technol.* **2021**, 29, e00304. [CrossRef]
- 77. Gan, Q.; Qin, N.; Zhu, Y.; Huang, Z.; Zhang, F.; Gu, S.; Xie, J.; Zhang, K.; Lu, L.; Lu, Z. Polyvinylpyrrolidone-Induced Uniform Surface-Conductive Polymer Coating Endows Ni-Rich LiNi_{0.8}Co_{0.1}Mn_{0.1}O₂ with Enhanced Cyclability for Lithium-Ion Batteries. *ACS Appl. Mater. Interfaces* **2019**, *11*, 12594–12604. [CrossRef]
- 78. Wang, H.; Lin, J.; Zhang, X.; Wang, L.; Yang, J.; Fan, E.; Wu, F.; Chen, R.; Li, L. Improved Electrochemical Performance of LiNi_{0.8}Co_{0.1}Mn_{0.1}O₂ Cathode Materials Induced by a Facile Polymer Coating for Lithium-Ion Batteries. *ACS Appl. Energy Mater.* **2021**, *4*, 6205–6213. [CrossRef]
- 79. Kaur, G.; Gates, B.D. Review—Surface Coatings for Cathodes in Lithium Ion Batteries: From Crystal Structures to Electrochemical Performance. *J. Electrochem. Soc.* **2022**, *169*, 043504. [CrossRef]
- 80. Lee, J.-E.; Kim, M.-C.; Moon, S.-H.; Kim, E.-S.; Shin, Y.-K.; Choi, S.; Kwon, S.-H.; Kim, S.-J.; Kwon, H.-J.; Park, K.-W. Role of polyvinylpyrrolidone in the electrochemical performance of Li₂MnO₃ cathode for lithium-ion batteries. *RSC Adv.* **2019**, *9*, 10297–10304. [CrossRef] [PubMed]
- 81. Li, Y.; Zhao, Y.; Cheng, H.; Hu, Y.; Shi, G.; Dai, L.; Qu, L. Nitrogen-Doped Graphene Quantum Dots with Oxygen-Rich Functional Groups. *J. Am. Chem. Soc.* **2012**, *134*, 15–18. [CrossRef]
- 82. Hu, S.; Huang, Q.; Lin, Y.; Wei, C.; Zhang, H.; Zhang, W.; Guo, Z.; Bao, X.; Shi, J.; Hao, A. Reduced graphene oxide-carbon dots composite as an enhanced material for electrochemical determination of dopamine. *Electrochim. Acta* **2014**, *130*, 805–809. [CrossRef]
- 83. Li, Z.; Liu, X.; Wang, L.; Bu, F.; Wei, J.; Pan, D.; Wu, M. Hierarchical 3D All-Carbon Composite Structure Modified with N-Doped Graphene Quantum Dots for High-Performance Flexible Supercapacitors. *Small* **2018**, *14*, 1801498. [CrossRef] [PubMed]
- 84. Lu, L.; Xie, Y. Phosphomolybdic acid cluster bridging carbon dots and polyaniline nanofibers for effective electrochemical energy storage. *J. Mater. Sci.* **2019**, *54*, 4842–4858. [CrossRef]
- 85. Wang, L.; Zeng, Q.; Chen, Q.; Li, C.M.; Chen, J. Synergistically boosting the electrochemical performance of polypyrrole-coated activated carbon derived from carbon dots for a high-performance supercapacitor. *Chem. Commun.* **2021**, *57*, 9264–9267. [CrossRef] [PubMed]
- 86. Xie, F.; Zhou, M.; Wang, G.; Wang, Q.; Yan, M.; Bi, H. Morphology-dependent electrochemical performance of nitrogen-doped carbon dots@polyaniline hybrids for supercapacitors. *Int. J. Energy Res.* **2019**, *43*, 7529–7540. [CrossRef]
- 87. Chen, J.; Li, F.; Gu, J.; Zhang, X.; Bartoli, M.; Domena, J.B.; Zhou, Y.; Zhang, W.; Paulino, V.; Ferreira, B.C.L.B.; et al. Cancer cells inhibition by cationic carbon dots targeting the cellular nucleus. *J. Colloid Interface Sci.* **2023**, *637*, 193–206. [CrossRef] [PubMed]

Disclaimer/Publisher's Note: The statements, opinions and data contained in all publications are solely those of the individual author(s) and contributor(s) and not of MDPI and/or the editor(s). MDPI and/or the editor(s) disclaim responsibility for any injury to people or property resulting from any ideas, methods, instructions or products referred to in the content.